IEEE Access
Multidisciplinary | Rapid Review | Open Access Journal

Received November 9, 2018, accepted November 19, 2018, date of publication December 6, 2018,
date of current version December 31, 2018.

Digital Object Identifier 10.1109/ACCESS.2018.2885118

Segment Particle Swarm Optimization Adoption for Large-Scale Kinetic Parameter Identification of *Escherichia Coli* Metabolic Network Model

MOHAMMED ADAM KUNNA AZRAG[1], TUTY ASMAWATY ABDUL KADIR[1], AND AQEEL S. JABER[2]

[1]Faculty of Computer Systems and Software Engineering, Universiti Malaysia Pahang, Kuantan 26300, Malaysia
[2]Department of Electrical Power Engineering Techniques, Almamon University College, Bagdad 1003, Iraq

Corresponding author: Mohammed Adam Kunna Azrag (mohammed87kunna@gmail.com)

This work was supported in part by the Ministry of Higher Education Malaysia and in part by Universiti Malaysia Pahang through FRGS under Grant RDU 160101.

ABSTRACT Kinetic parameter identification in the dynamic metabolic model of *Escherichia coli (E. coli)* has become important and is needed to obtain appropriate metabolite and enzyme data that are valid under *in vivo* conditions. The dynamic metabolic model under study represents five metabolic pathways with more than 170 kinetic parameters at steady state with a 0.1 dilution rate. In this paper, identification is declared in two steps. The first step is to identify which kinetic parameters have a higher impact on the model response using local sensitivity analysis results upon increasing each kinetic parameter up to 2.0 by steps of 0.5, while the second step uses highly sensitive kinetic results to be identified and minimized the model simulation metabolite errors using real experimental data by adopting. However, this paper focuses on adopting segment particle swarm optimization (PSO) and PSO algorithms for large-scale kinetic parameters identification. Among the 170 kinetic parameters investigated, seven kinetic parameters were found to be the most effective kinetic parameters in the model response after finalizing the sensitivity. The seven sensitive kinetic parameters were used in both the algorithms to minimize the model response errors. The validation results proved the effectiveness of both the proposed methods, which identified the kinetics and minimized the model response errors perfectly.

INDEX TERMS System biology, metabolic model, sensitivity analysis, identification, PSO, Se-PSO.

I. INTRODUCTION

The study of system biology involves integrating computational modeling with experimental methods in order to better understand the behavior of living organisms, the regulation of their cellular processes, and how these cells react to environmental perturbations [1]. Computational modeling has been used to study enzyme activities, metabolic concentration, and kinetic parameters impact [2], [3]. In addition, kinetic modeling in system biology gives the most detailed representation of the biological system. This model builds on the stoichiometry of the reactions, incorporating the dynamic interactions between different components of the network [1]. A dynamic model of the metabolic network is explained by the metabolic concentration and activity of the enzyme with respect to time. This dynamic model can be described by nonlinear ordinary differential equations (ODEs) derived from the mass-balance equation of metabolites related to the enzymatic reaction [4]. The enzymatic reactions have large kinetic parameters of the main metabolic dynamic model that need to be identified [5]. Each dynamic metabolic physiology has a set of parameters, such as temperature, reaction rates, metabolites and kinetic constants [6], [7]. The kinetic parameters strongly support building an accurate dynamic metabolic system that represents the main metabolic model of *E. coli*. The kinetic parameters are mostly estimated or reported from different laboratories and are difficult to identify if extracted from experimental data [2], [6]. However, the challenges faced during the building of the dynamic model are stated in four steps: i) defining the structure of the model, ii) formulating the kinetic rate equation, iii) defining the parameter identification/estimation of unknown parameters, and iv) increasing the understanding of the regulatory structure system [8], [9]. Gábor *et al.* [4] stated that the necessary estimation of the dynamic model kinetic parameters has

four faces: i) the often practically unidentifiable nature of some of the kinetics, which cannot be uniquely determined from the available data, ii) the lack of influence on the measures response, and iii) the poor data quality. Yet, there are two class of identification/estimation methods: i) numerical ordinary differential equations solver which is employed to simulate the trajectory and the derivative of the ODEs models, while an optimization algorithm is applied to identify/estimate the unknown parameters; ii) decoupling approaches which reformulates the system by incorporating differential equations into a system of algebraic equations to relieve the computational burden [10]. In addition, the problem of identification/estimation of parameters of nonlinear problems has been known to be multimodal and difficult due to the rare information in the available data [11].

Moreover, the study of dynamic metabolic *E. coli* currently has become very significant in medicine and chemistry due to its important production. To study the cell behavior of *E. coli*, we need to understand and study the metabolic engineering, which leads to the expansive gathering of computational tools to utilize and assist in the rational engineering of the cellular metabolism when controlling, analyzing, and visualizing large pathways [11]. Large pathways need large kinetic parameters, which have been studied and analyzed to detect the concentration of changes in the metabolites and reactions using ordinary differential algebraic equations [12].

Since 2002, the analytical studies of the sensitivity analysis and parameter identification/estimation have been used for three pathways in kinetic modeling. Chassagnole *et al.* [13] investigated the glycolysis and pentose phosphate pathways by applying a stepwise internalization method for the sensitivity analysis and used simulating annealing to optimize 85 kinetics that represented his model. In the work of Di Maggio *et al.* [14] stated that twelve kinetic parameters were identified as effective parameters for the Embden-Meyerhof pathway, pentose phosphate pathway, and phosphotransferase system. They used Monte Carlo simulation and the Sobol method for calculating the time profiles. Nine of the most sensitive kinetic parameters have been optimized through the Control Vector Parameterization Approach to formulate the dynamic parameter estimation problems [13], [14]. Therefore, the least squares techniques and Real-coded Genetic Algorithm were used to fit the model output to the corresponding experimental measurements that Tohsato *et al.* [12] applied. They applied the sensitivity analysis to 100 kinetics by scaling each kinetic parameter individually from 0.0 up to 2.0 by step 0.2. Seven kinetic parameters were stated as the most significant parameters, considering v^{max} as a kinetic target in the Real-coded Genetic Algorithm, which was used for optimization of the experimental data [10] taken from a previous study [13].

The Genetic Algorithm (GA) procedure has lately been evaluated for estimating the kinetic parameters involved in bio-surfactant production from agro-industrial waste; 3 ODEs were used while 7 kinetic parameters were calculated [15]. Also [2], four objective functions were investigated on the influence of the number of unknown parameter on the convergence through a comparison of data driven from simulation with data from factor scaling. The genetic local search algorithm with distance independent diversity control (GLSDC), coupled with Levenbreg-Marquardt nonlinear least squares optimization algorithm (LevMar) were implemented. As mentioned previously, the parameter boundaries selection was not stated, and this is why parameter segmentation is proposed in this study to minimize the boundaries search space. However, Particle Swarm Optimization (PSO) is a relatively new family of algorithms that may be used to determine the optimal solution to the high complexity or multidimensional functions [16]. To this point, they stated that 7 kinetic parameters were identified using a One-At-A-Time sensitivity measure, and 4 metabolites were optimized using the PSO algorithm due to the lack of experimental data and focus in the two pathways only to determine the complexity of the ODE solution [17]. The algorithm of PSO emulates from the behavior of animal societies that do not have any leader in their group or swarm, such as birds flocking and fish schooling [18]. The PSO algorithm contains many different mechanisms that improve global and local exploration abilities [19], [20]. From the implementation of GA and PSO algorithms in the estimation of growth kinetic parameters in fermentation processes, PSO was observed to provide a better convergence compared to GA [21]. In addition, PSO algorithm is sufficient in reducing the steady-state errors [22] than the other algorithms such as Genetic Algorithm and Simulating Annealing where sensitivity analysis should be performed at a steady-state condition (the sensitive kinetic parameters can be addressed at this point). Additionally, the observed behavior of a system in a steady state will continue to be observed in the future. Due to the ability of the PSO algorithm to find high solutions in nonlinear systems, many researchers proposed to improve the accuracy and time consumption for large nonlinear models, such as the hybrid Artificial Bee Colony (ABC) and PSO to modify the continuous functions [23], [24] and the Segmentation of the PSO algorithm to identify the governor-turbine system model [22]. The new segmentation of the PSO algorithm was proposed to identify large-scale kinetic parameters and minimize the model response of the main dynamic metabolic model of *E. coli* pathways. Moreover, the segmentation process provides sufficient information for kinetic parameters and minimizes the kinetic boundaries. This study focuses on applying local sensitivity analysis to study, analyze, and investigate the large-scale kinetic parameters of the main metabolic model of *E. coli* formulated by [25]. The sensitivity analysis was performed by increasing each Kinetic parameter to 50 %, 100 %, 150 % and 200 % based on the recommendation provided by [12]. In addition, a new method called Segment Particle Swarm Optimization was proposed in this study to select the kinetic boundaries to be identified after stating the outcome of the sensitivity analysis based on real experimental data. Moreover, the result of the proposed algorithm was compared to the Particle Swarm

Optimization Algorithm result in terms of accuracy and time consumption. Therefore, 7 metabolites concentration was moved toward the experimental data in both algorithms. Among the 7 metabolites, 2-Keto-D-gluconate (2KG) in Se-PSO algorithm moved almost twice towards the experimental data than PSO algorithm. In addition, the identified computational effort by Se-PSO was 21 hours while PSO was 23 hours. However, it proved that the adoption of Se-PSO and PSO algorithms for large-scale identification was highly effective in identifying the kinetic parameters and minimizing the model error response within a shorter time.

II. METHODS

This research has three parts. The first part presents a brief description of the metabolic model structure; the second part explains the methodologies of the sensitivity analysis with the PSO algorithm and the new Se-PSO algorithm adoption; while the third part is the analysis, the results and validation of the proposed methods.

A. MODEL STRUCTURE

Each metabolic model contains pathways; these pathways are described by a series of chemical reactions occurring within the cell [26]–[28]. However, the main metabolic pathway model of *E. coli* formulated by [25] was considered a benchmark. This model describes the dynamic metabolic behavior of the Glycolysis, Pentose Phosphate, Tricarboxylic Acid Cycle (TCA), Gluconeogenesis, and Glyoxylate pathways, in addition to acetate formation pathway which contains 23 metabolites and 28 enzymatic reactions with 10 co-factors, including NAD, CoA, ATP.

In addition, the metabolites of Glyceraldehyde 3-Phosphate (*GAP*) and Dihydroxyacetone Phosphate (*DHAP*) were lumped together. This lump considers the enzymatic reaction of Glyceraldehyde 3-Phosphate Dehydrogenase- Dihydroxyacetone Phosphate (*gapdh*), Pyruvate Kinase (*pyk*), Phosphoglucomutase (*pgm*) and Enolase (*eno*) to be in equilibrium and assumed one reaction from Glyceraldehyde 3-Phosphate (*GAP*) to Phosphoenol-Pyruvate (*PEP*) for simplicity purposes [25]. The corresponding metabolic network is shown in Figure 1 below. The metabolite concentration rate of the changes in this metabolic network is given by Equation (1):

$$\frac{dc_i}{dt} = \sum R_{ij} v_j - \mu C_i \tag{1}$$

where C_i is the concentration of metabolite i, R_{ij} is the stoichiometric coefficient of metabolite i in reaction j, v_j is the rate of the reaction j and μC_i is the growth rate on the dilution effect. All formulas and mass balance in this dynamic model are taken from [25]. The kinetic rate equation is described in Appendix while the mass balance equations of the model under study were described in Table 1.

B. THE IDENTIFICATION IMPLEMENTATION

The identification implementation depends on the sensitivity analysis and optimization algorithm. In the sensitivity

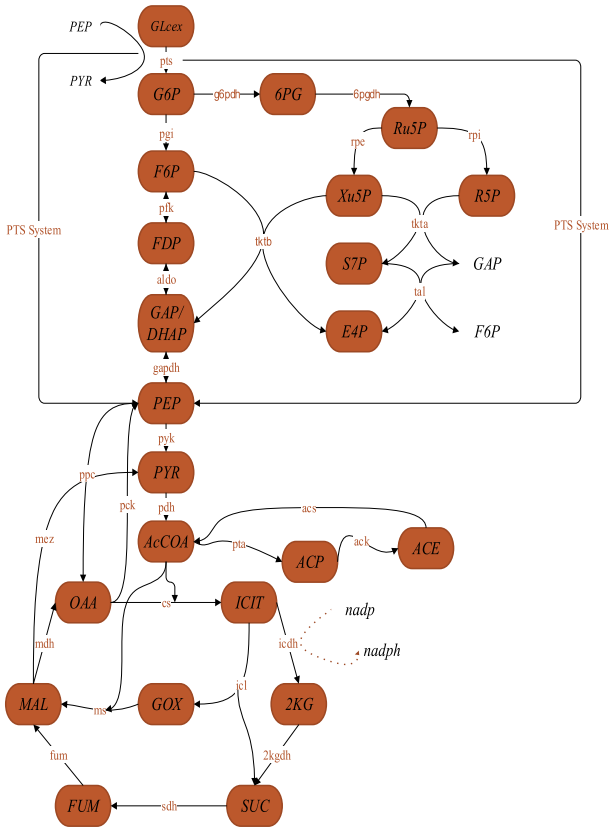

FIGURE 1. The main metabolic network of *E. coli*.

analysis where the results of [19] were used to achieve the identification of large scale kinetic parameters, these parameters were investigated again by increasing each kinetic parameter by 50, 100, 150 and 200 % from the original kinetic parameters based on [12] the measured at the steady-state condition to enhance the result. The increasing or decreasing in the model response after applying sensitivity in each kinetic was calculated based on the percentage changes to identify the most sensitive kinetics using Equation (2):

$$Sensitivity\ of\ k = \left(\frac{R_{mi} - R_{si}}{R_{mi}}\right) \%100 \tag{2}$$

where k is the kinetic parameter, the R_{mi} is the model metabolite that resulted from the mi model and R_{si} is the simulation metabolite result for the si model.

Normally, the identification of the kinetic parameter techniques in the optimization algorithms is based on the difference between the simulated model and the actual system model behavior to minimize the model simulation errors [13] based on the sensitivity analysis result. However, the function used to identify the large-scale kinetic parameter metabolic network of the *E. coli* system model is transferred as Equation (3):

$$fitness = |(R_{s1} - R_{m1}) + (R_{s2} - R_{m2}) + \ldots + (R_{si} - R_{mi})| \tag{3}$$

TABLE 1. The mass balance equations.

Metabolites	Mass balance description
Cell (X)	$\frac{d[X]}{dt} = \mu[X]$
Extra Glucose (GLC^{ex})	$\frac{d[GLC^{ex}]}{dt} = -v_{PTS}[X]$
Glucose-6-phosphate (G6P)	$\frac{d[G6P]}{dt} = v_{PTS} - v_{PGI} - v_{G6PDH} - \mu[G6P]$
Fructose 6-phospahte (F6P)	$\frac{d[F6P]}{dt} = v_{PGI} - v_{PFK} + v_{TKTB} + v_{TAL} - \mu[F6P]$
Fructose 1,6-Phosphate (FDP)	$\frac{d[FDP]}{dt} = v_{PFK} - v_{ALDO} - \mu[FDP]$
Glyceraldehyde 3-phosphate (GAP)	$\frac{d[GAP]}{dt} = 2v_{ALDO} - v_{GAPDH} + v_{TKTA} + v_{TKTB} - v_{TAL} - \mu[GAP]$
Phosphoenol-pyruvate (PEP)	$\frac{d[PEP]}{dt} = v_{GAPDH} + v_{PCK} - v_{PTS} - v_{PYK} - v_{PPC} - \mu[PEP]$
Pyruvate (PYR)	$\frac{d[PYR]}{dt} = v_{PYK} + v_{PTS} + v_{MEZ} - v_{PDH} - \mu[PYR]$
Acetyl-CoA (AcCoA)	$\frac{d[AcCoA]}{dt} = v_{PDH} + v_{ACS} + v_{CS} - v_{PTA} - \mu[AcCoA]$
Isocitrate (ICIT)	$\frac{d[ICIT]}{dt} = v_{CS} - v_{ICDH} - v_{ICL} - \mu[ICIT]$
2-Keto-D-gluconate (2KG)	$\frac{d[2KG]}{dt} = v_{ICDH} - v_{2KGDH} - \mu[2KG]$
Succinate (SUC)	$\frac{d[SUC]}{dt} = v_{2KGDH} + v_{ICL} - v_{SDH} - \mu[SUC]$
Fumarate (FUM)	$\frac{d[FUM]}{dt} = v_{SDH} - v_{FUM} - \mu[FUM]$
Malate (MAL)	$\frac{d[MAL]}{dt} = v_{FUM} + v_{MS} - v_{MDH} - v_{MEZ} - \mu[MAL]$
Oxaloacetate (OAA)	$\frac{d[OAA]}{dt} = v_{MDH} + v_{PPC} - v_{CS} - v_{PCK} - \mu[OAA]$
Glyoxylate (GOX)	$\frac{d[GOX]}{dt} = v_{ICL} - v_{MS} - \mu[GOX]$
Acetyl phosphate (ACP)	$\frac{d[ACP]}{dt} = v_{PTA} - v_{ACK} - \mu[ACP]$
Acetate (ACE)	$\frac{d[ACE]}{dt} = (v_{ACK} - v_{ACS})[X]$
6-Phosphogluconolactone (6PG)	$\frac{d[6PG]}{dt} = v_{G6PDH} - v_{6PGDH} - \mu[6PG]$
Ribose 5-phosphate (Ru5P)	$\frac{d[Ru5P]}{dt} = v_{6PGDH} - v_{RPE} - v_{RPI} - \mu[Ru5P]$
Ribulose 5-phosphoenolpyruvate (R5P)	$\frac{d[R5P]}{dt} = v_{RPI} - v_{TKTA} - \mu[R5P]$
Xylulose 5-phsophate (Xu5P)	$\frac{d[Xu5P]}{dt} = v_{RPE} - v_{TKTA} - v_{TKTB} - \mu[Xu5P]$
Sedoheptulose 7-phosphate (S7P)	$\frac{d[S7P]}{dt} = v_{TKTA} - v_{TAL} - \mu[S7P]$
Erythrose 4-phsophate (E4P)	$\frac{d[E4P]}{dt} = v_{TAL} - v_{TKTB} - \mu[E4P]$

where R_{mi} is the model metabolite that resulted for the *mi* model and R_{si} is the simulation metabolite that results for the *si* model. However, the PSO and Se-PSO algorithms were presented below.

C. PSO ADOPTION ALGORITHM

Eberhart and Kennedy in 1995 proposed a new heuristic method called the Particle Swarm Optimization [18]. This algorithm was inspired by the social behavior of bird flocking or fish schooling, and shares many similarities with evolutionary techniques, such as Genetic Algorithm, Simulating Annealing, and Artificial Neural Network. In the PSO, the potential solution was called the particles search in the problem space by following the current optimum particles. In order to adopt PSO in the dynamic model of *E. coli*, the kinetic parameter sensitivity result of the [25] model will be initialized. Secondly, seven kinetic parameters value ranges were adopted by setting the upper and lower value of each parameters with respect to the fitness function because the solution is multifunctionally searched near or equal to zero using Eq 3. Thirdly, the experimental data from [29] was initialized and the fitness function calculation using Eq 3 above with respect to the model simulation that contains the equations of the ODE function was adopted. During the PSO execution, the maximum number of the generation is set at 100 (bird-steps), the dimension's problem is 7 kinetic parameters, the population size (iterations) was repeated 500 times, the linear inertia weight was 0.9, and the PSO parameter $c_1 = 1.5$ and $c_2 = 0.8$ had lower and upper values for each kinetics. PSO was inspired by the food-searching behaviors of fish and their activities or a flock of birds in the D-dimensional search space, and the best individual position of particle *i* and the best position of the entire swarm are represented by [22] and [30] and described in Eq 4 & 5 below.

$$v_i(t+1) = \omega v_i(t) + c_1 r_1 (p_i(t) - X_i(t)) + c_2 r_2 (G_i(t) - X_i(t)) \quad (4)$$

$$X_i(t+1) = X_i(t) + v_i(t+1) \quad (5)$$

Where p_i is the best position already found by particle *i* until time *t* and *G* is the best position already found by particle *i* until time *t*, and ω is an inertia weight parameter to explore search space. Additionally, c_1, c_2 are acceleration coefficients toward *P* and *G*, respectively, and r_1, r_2 are random numbers between 0 and 1. In each iteration, the particles will use Eq 3 & 4 to update their position (X_i) and velocity (V_i), and the algorithm adoption used in this work is described below.

The above PSO adoption algorithm was described by initializing the particles, which are the maximum number of generation *S*, a number of bird steps *B*, problem dimension *D*, and inertia weight ω in step 2. Then, in step 3 the parameters of PSO were initialized, which are acceleration coefficients toward the best personal position p_i and the global best position of the entire G_i respectively, where (c_1&c_2) are random numbers between 0 and 1 for (r_1, r_2). For each particle *i*, the number of bird step *B* was set. The kinetics

Algorithm 1 PSO Algorithm Adoption

1 BEGIN
2 initialize *S, B, D,* ω;
3 initialize $v_i, X_i, c_1, c_2, r_1, r_2$;
4 adopt the $b_{e1} : b_{en}$ parameters boundaries with respect to D.
5 For *m* data account:

$$fitness = \left| \begin{array}{l} (R_{s1} - R_{m1}) + (R_{s2} - R_{m2}) \\ + \ldots + (R_{si} - R_{mi}) \end{array} \right|$$

6 If $fitness > 0$
7 For each *S*;
8 iter $S = 1, S{+}{+}$;
9 Updating the velocity V_i toward fitness: $v_i(t+1) = \omega v_i(t) + c_1 r_1 (p_i(t) - X_i(t)) + c_2 r_2 (G_i(t) X_i(t))$
Update the position X_i toward fitness: $X_i(t+1) = X_i(t) + v_i(t+1)$
10 If fitness ≤ 0,
Print $G_i best$ of each particles;
11 If fitness $>$ 0 return step 2 till the iteration is finished or discover high-quality solution;
12 End

$b_{e1} : b_{en}$ boundaries for problem dimension *D* were adopted. In step 5, the fitness function is adopted using absolute values to minimize the model metabolite simulation R_{si} with real experimental data R_{mi} using the kinetics calculation inside the model to achieve minimization. The procedure calculation toward the identification is started by iteration *S* in step 6 and 7. The particle velocity and position are updated to adjust the particle movement toward the fitness function in step 8 and 9. If the previous steps prove that the fitness function is less than or equal to zero, then the global best position of each particle in step 10 was printed. If the fitness function is greater than zero, then we returned to step 2 till the maximum number of generations is end or the solution is discovered in step 11.

D. Se-PSO ADOPTION ALGORITHM

The PSO algorithm was introduced by Eberhart and Kennedy as a new heuristic method [16], [17]. PSO was inspired by the food-searching behaviors of fish and their activities or a flock of birds in D-dimensional search space, with the best individual position of particles and the best position of the entire swarm [22]. The idea of the Segmentation PSO algorithm is to divide the initial values into segments and help the PSO particles during the search for optimal values, finding the local best position and the global best position may be around it. The segmentation can be divided in more than two groups based on the dimension problem [23]. Each group of particles was considered as a segment, while the procedures for finding the optimal solution (optimal segments) follow the PSO algorithm; then, the optimal segment for the initial parameters will be used as the new initial parameters later

in the PSO search, ranging toward the optimal solution. The segmentation can be described in Figure 2 below.

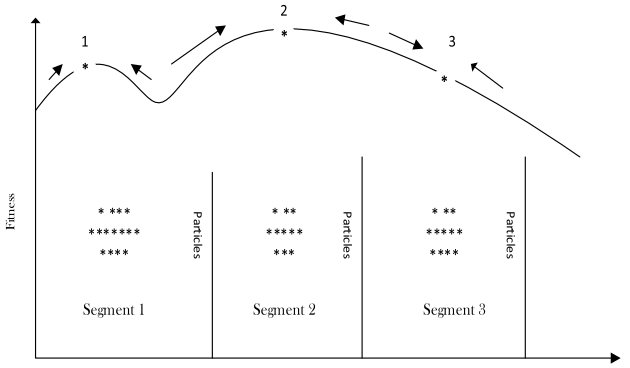

FIGURE 2. The segmentation procedure.

In the above Figure, the segments easily located many local points, where point 2 is the best local point, as the best individual position of the particle and the best position of the entire swarm should be modified to achieve the best optimal segment as follows in Eq 6:

$$Seg\ length = \frac{initial\ limits}{number\ of\ segments} \tag{6}$$

Then, equation 3 should be modified according to the segmentation changes and described as follow in Eq 7 & 8:

$$v_i(t+1,j) = \omega v_i(t,j) + c_1 r_1(p_i(t,j) - X_i(t,j)) + c_2 r_2(G_i(t,j) - X_i(t,j)) \tag{7}$$

$$X_i(t+1,j) = X_i(t,j) + v_i(t+1,j) \tag{8}$$

Hence the optimal segment can be described in Eq 9:

$$optimal\ segment = \frac{optimalX_{ij} \mp segment\ length}{2} \tag{9}$$

where j is the number of segments.

To initialize the kinetic parameter sensitivity of the [25] model result inside the Se-PSO algorithm. First, the seven kinetic parameters value boundaries were adopted by setting the upper and lower value of each parameter with respect to the fitness function, then the kinetic parameters were divided into segments based on the sensitivity analysis result on the model response. Second, the experimental data from [29] was initialized and the fitness function calculation using the *Eq 2* above was adopted with respect to model simulation, containing ODE function. During Se-PSO execution, the maximum number of generations was set as 5 (bird-steps), the dimension problem is 7 kinetic parameters, the population size (iterations) was repeated 30 times, the linear inertia weight was 0.9, and the PSO parameter $c_1 = 1.2$ and $c_2 = 1.2$ with lower and upper values for each kinetics. The algorithm adoption used in this work will be described below.

The above Se-PSO adoption algorithm was described by initializing the particle, which is the maximum number of generations $S = 30$, $b_{e1} : b_{en}$ is the kinetic boundaries b from $e1$ $toe7$, the problem dimension $D = 7$, and inertia

Algorithm 2

1 BEGIN
2 Initialize S, D, ω;
3 initialize v_i, X_i, c_1, c_2, r_1, r_2, number_segment;
4 Segment length=initial value/number_segment;
5 Adopt the $b_{e1} : b_{en}$ parameters boundaries with respect to D;
6 For j = 1 to number of segment;
7 Determine initial *fitness* for segment J;
8 Assume *Best fitness* = *initial fitness*;
For m data account:

$$fitness = \left| \begin{matrix} (R_{s1} - R_{m1}) + (R_{s2} - R_{m2}) \\ + \ldots + (R_{si} - R_{mi}) \end{matrix} \right|;$$

9 End for,
10 If *fitness* > Best *fitness*;
11 For each S;
12 iter $S = 1, S++$;
13 Updating the velocity V_i toward fitness: $v_i(t+1,j) = \omega v_i(t,j) + c_1 r_1(p_i(t,j) - X_i(t,j)) + c_2 r_2(G_i(t,j) X_i(t,j))$;
14 Update the position X_i,j toward fitness: $X_i(t+1,j) = X_i(t,j) + v_i(t+1,j)$;
15 End if,
16 If fitness ≤ Best *fitness*;
Print $G_i best$ of each particles;
Update the $b_{e1} : b_{en}$ based of $G_i best$ of each kinetic parameters;
17 If fitness > Best *fitness* return step 2 till the iteration is finished or discover high-quality solution;
18 End if,
19 End if,
20 Global point(j) = $G_i best$;
21 Next, j;
22 Optimal_segment=max (Global point) ± segment length/2;
23 Repeat algorithm 1 for the new initial values;
24 End.

weight $\omega = 0.9$ in step 2. Then, in step 3, the parameters of PSO were initialized, which are acceleration coefficients toward the best personal position p_i and the global best position of the entire G_i, where (c_1&c_2) are random number between 0 and 1 for (r_1, r_2) in addition to the segment number of the bird step of Se-PSO = 5. The segment length was calculated using step 4. The boundaries (upper/lower) of each kinetic parameter were created with respect to the dimension problem D in step 5. Based on the number of segments, the initial fitness of the whole segments was calculated assuming that initial fitness is the best fitness step 6, 7, and 8.

However, the new fitness was calculated based on the fitness equation stated in step 9. If the fitness was greater than the best fitness set iteration, the velocity and position was calculated toward the new fitness step 11, 12, 13, 14 and 15.

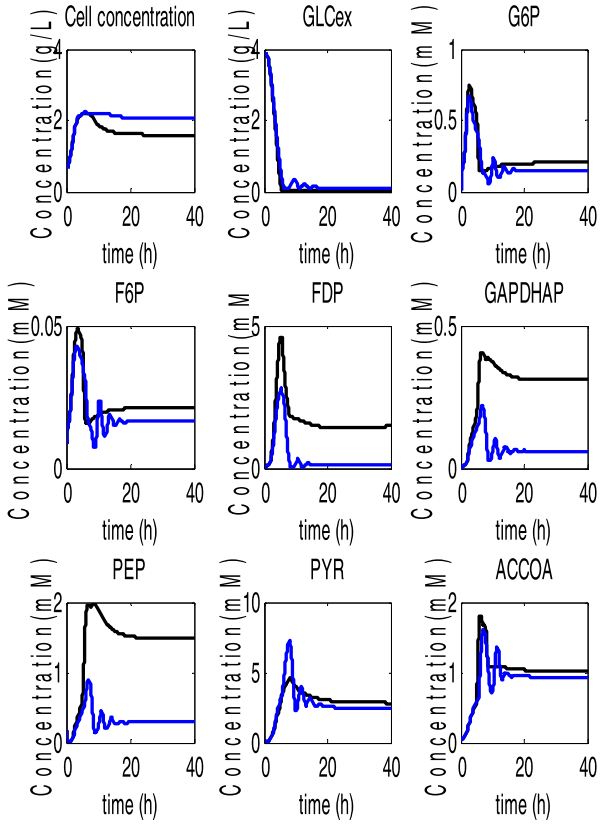

FIGURE 3. v_{max}^{pyk} changes on the model response.

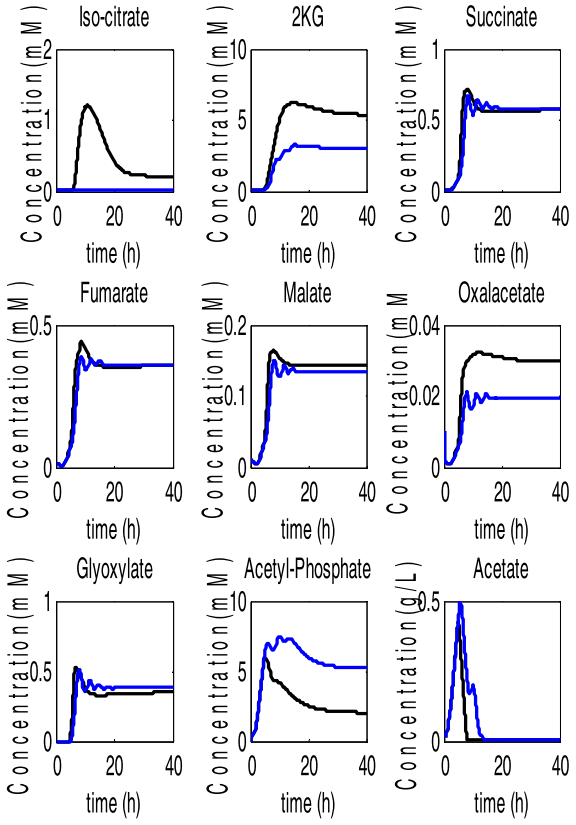

FIGURE 4. v_{max}^{pyk} changes on the model response.

If the new fitness was smaller than or equal to the best fitness print, the global best particle position and the kinetic parameter update based on the global best particle position was used as the new initial kinetic parameters step 17. If fitness is greater than the best fitness returns in step 2, the program figured out the solution or the iteration, which is met in step 18.

The global point of the segments equal to the global best position were then used to calculate the optimal segment by equation 21, 22, and 23. After the optimum segments were identified, they were used as the new initial kinetic parameter and PSO algorithm, which will search among them until the end of the program in step 24.

III. RESULTS

The large-scale kinetic parameters identification was achieved by applying sensitivity analysis, adopting PSO with new Se-PSO algorithms as the primary target of this study. However, the sensitivity analysis result shows that there are 7 kinetic parameters affecting the model response, while the PSO and Se-PSO algorithms identified and minimized these parameters to achieve better model response errors as discussed below.

A. SENSITIVITY ANALYSIS

The sensitivity analysis for all the kinetic parameters was used based on [25] model with a 0.1 dilution rate to

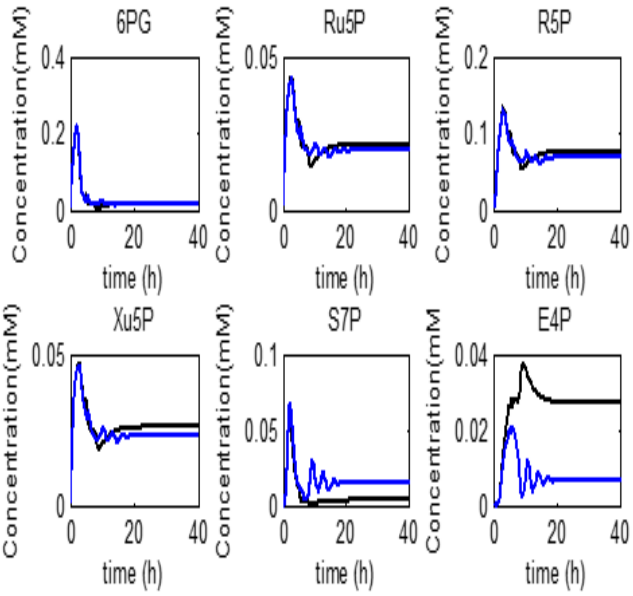

FIGURE 5. v_{max}^{pyk} changes on the model response.

be investigated. The kinetic parameter results of [5], which are v_{max}^{pyk}, n_{pk}, $icdh$, k_{icdh}^{f}, $k_{icdhnadp}^{d}$, $k_{icdhnadp}^{m}$, and v_{max}^{icl}, were involved in the reaction rates of V_{pyk}, V_{icdh}, *and* V_{icl} and used as a benchmark. These kinetic parameters were used to minimize the error in the metabolite model simulation result,

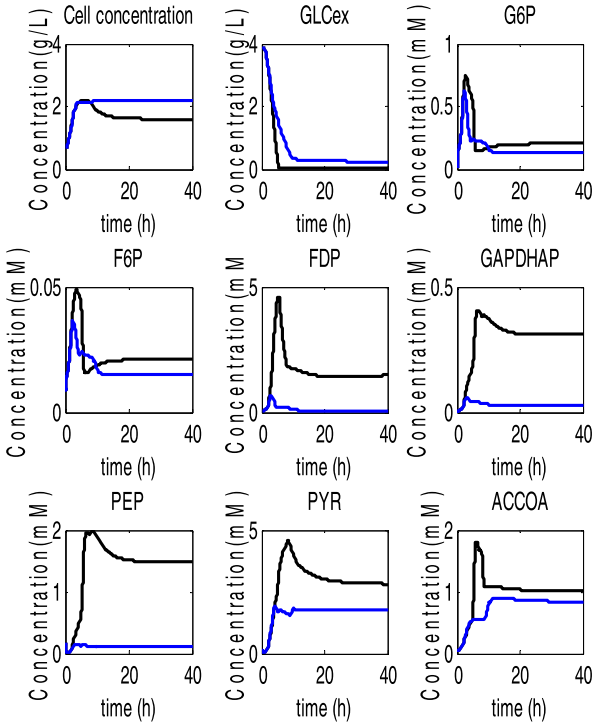

FIGURE 6. n_{pk} changes on the model response.

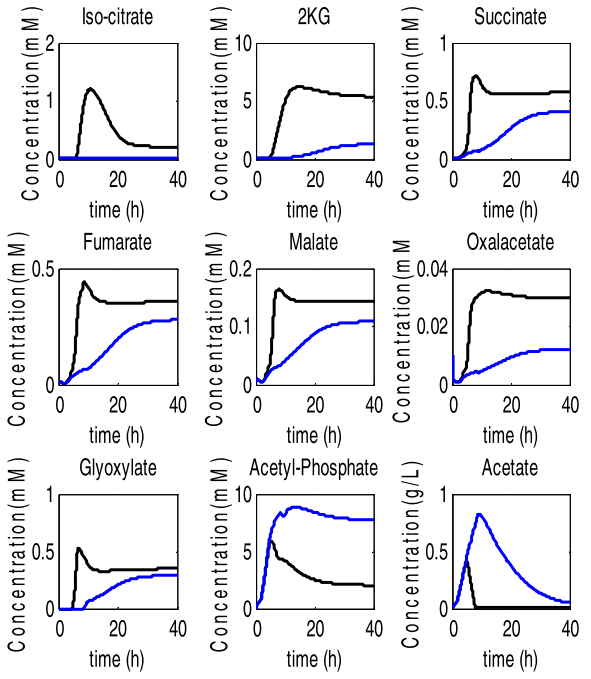

FIGURE 7. n_{pk} changes on the model response.

with the experimental data taken from [25]. The rest of the kinetic parameters had slight effects.

However, the analysis of the kinetic parameters on the model response has been described below with the blue line increasing each kinetic parameter 50%, 100%, 150% to 200% to enhance the last sensitivity analysis result of [17] based

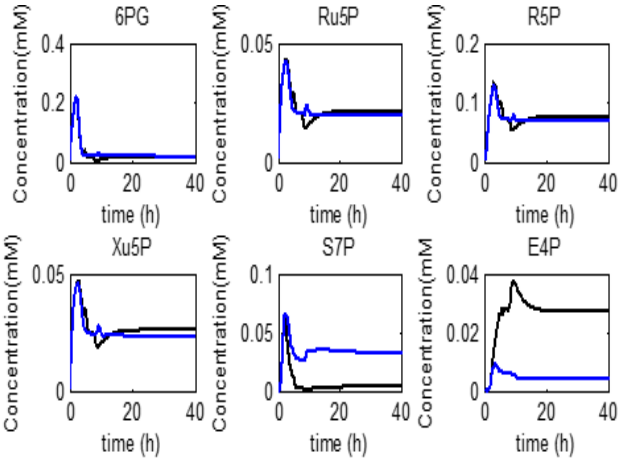

FIGURE 8. n_{pk} changes on the model response.

on [12], where the changes of the 7th kinetics are shown below for 200% because the affection is the same as increasing the others 50-200%. The sensitivity was described in the blue line, while the model was described in the black line.

The changes in the value of v_{max}^{pyk} causes increases in the *cellconcentration*, *PYR*, *S7P*, *ACE* and *ACP* while decreasing in *F6P*, *FDP*, *GAP/DHAP*, *PEP*, *ICIT*, *2KG*, *OAA*, and *E4P*. This might be due to the anaplerotic pathway involvement in PEP and PYR, or the PTS affection on PEP or the $PykI - PykII$ iso-enzymes, which catalyzed the reaction of *Pyk*, where *PykI* is activated by *FDP* and inhabited by *ATP* and *PykII*, which is activated by *AMP* [25], where the changes are described in Figure 3, 4, and 5.

The n_{pk} kinetic parameter changes on the model response causes increases in *Glcex*, *ACE*, *ACP*, and *S7P*, while decreasing *G6P*, *F6P*, *FDP*, *GAP/DHAP*, *PEP*, *PYR*, *AcCOA*, *ICIT*, *2KG*, *SUC*, *FUM*, *MAL*, *OAA*, *GOX*, and *E4P*, as described in Figures 6, 7, and 8 below.

The *icdh* kinetic parameter changes on the model response causes increases in the metabolites of *PYR*, *AcCOA*, and *ACP* while causing decreases in the metabolites of *FDP*, *GAP/DHAP*, *PEP*, *ICIT*, *2KG*, *SUC*, *FUM*, *MAL*, *OAA*, *GOX*, and *E4P*. This affection might be caused by the reaction of *GAPDH*, which is assumed to inhibit *NADH* as the $[\frac{NADH}{NAD}]$ ratio increases [13]; the affections are described in Figures 9, 10, and 11 below.

The k_{icdh}^{f} kinetic parameter changes on the model responses causes increases in the metabolites of *PYR*, *AcCOA*, and *ACP* while causing decreases in the metabolites of *FDP*, *GAP/DHAP*, *PEP*, *ICIT*, *2KG*, *SUC*, *FUM*, *MAL*, *OAA*, *GOX*, and *E4P*, as described in Figures 12, 13, and 14 below.

The $k_{icdhnadp}^{d}$ kinetic parameter changes on the model response causing increases in the metabolites of *PYR*, *AcCOA*, and *ACP*, while causing decreases in the metabolites of *FDP*, *GAP/DHAP*, *PEP*, *ICIT*, *2KG*, *SUC*, *FUM*, *MAL*, *OAA*, *GOX*, and *E4P* as described in Figure 15, 16, and 17 below:

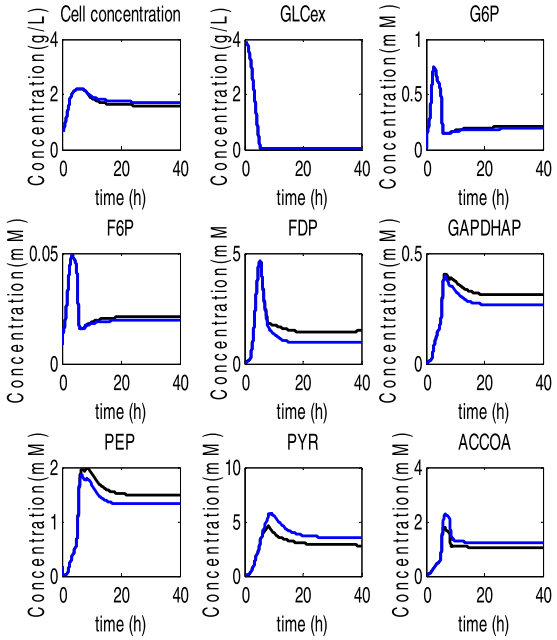

FIGURE 9. *icdh* changes on the model response.

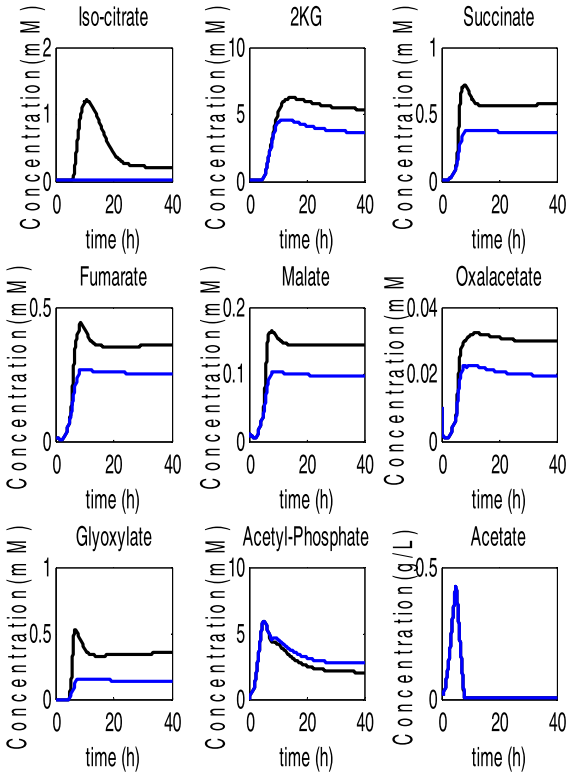

FIGURE 10. *icdh* changes on the model response.

The $k^{m}_{icdhnadp}$ kinetic parameter changes on the model response causes increases in the metabolites of $F6P$, FDP, $GAP/DHAP$, $ICIT$, SUC, FUM, MAL, GOX, and $E4P$, while causing decreases in the metabolites of PYR, $AcCOA$, $2KG$, OAA and ACP as described in Figure 18, 19, and 20 below:

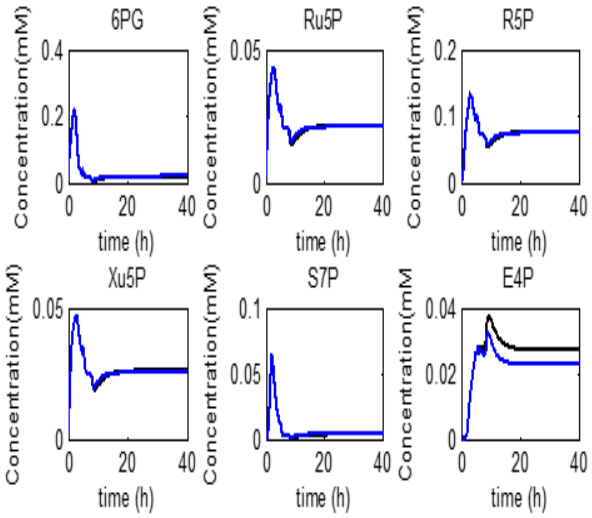

FIGURE 11. *icdh* changes on the model response.

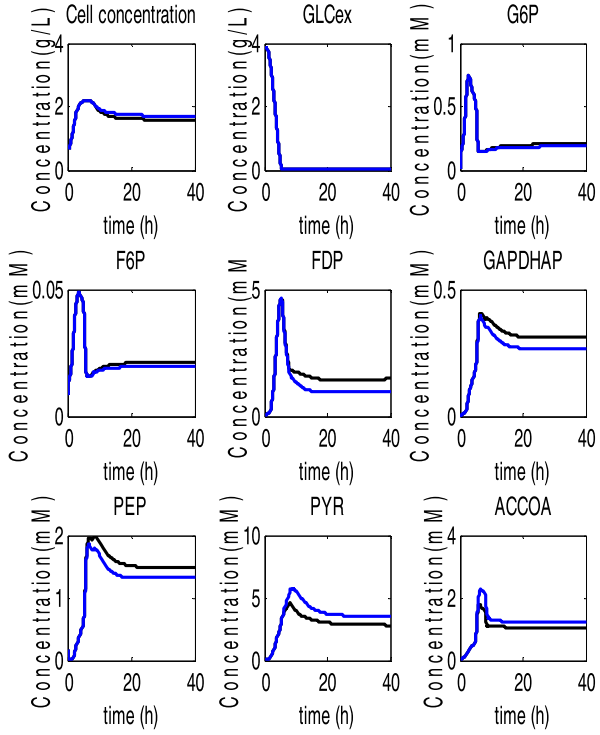

FIGURE 12. k^{f}_{icdh} changes on the model response.

The v^{icl}_{max} kinetic parameter changes in the model response causes increases in the metabolites of $F6P$, FDP, $GAP/DHAP$, PEP, $2KG$, SUC, FUM, MAL, OAA, GOX and $E4P$ while causing highly causing decreases in the metabolites of PYR, $AcCOA$, $ICIT$ and ACP, which might be due to $icl - ICIT$ being the reaction substrate, which is inhibited by the high accumulation of its products of SUC and GOX described in Figures 21, 22, and 23 below:

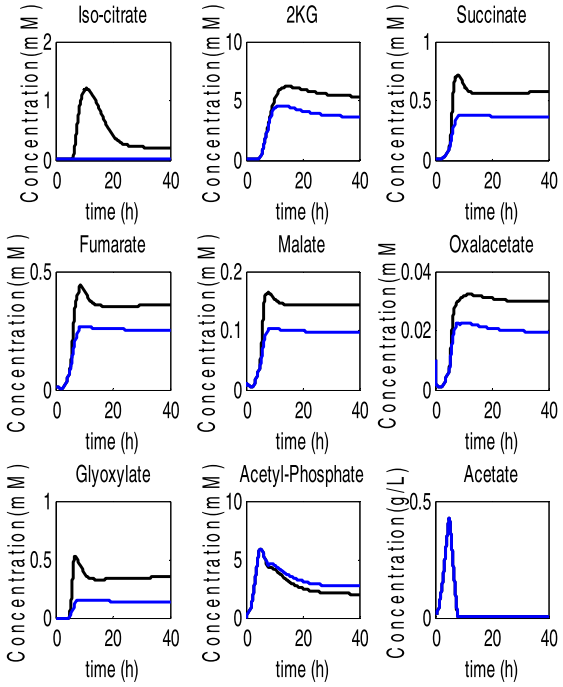

FIGURE 13. k^{f}_{icdh} affection on the model response.

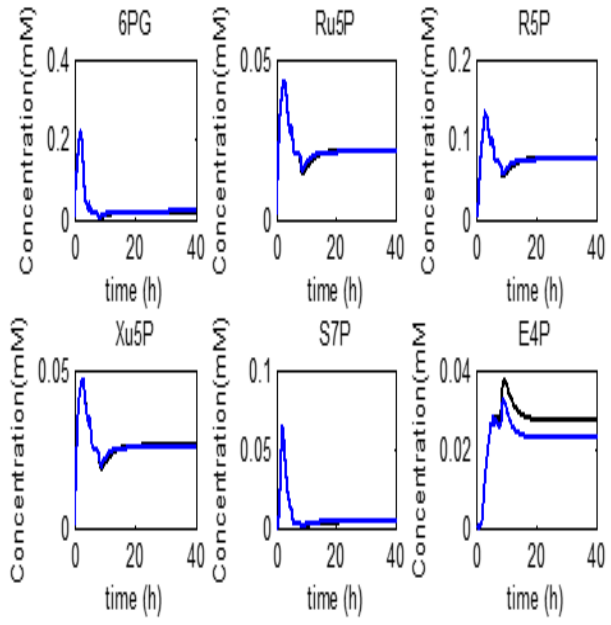

FIGURE 14. k^{f}_{icdh} changes on the model response.

B. THE PSO RESULT

In the PSO algorithm, the whole mass balance equations and reaction rates, including the whole kinetic parameters, were adopted. The seven parameter boundaries were adopted based on the kinetic parameter simulation values of the model under study and should be found during PSO execution toward model minimization. During PSO adoption execution, the calculation values of each parameter were calculated

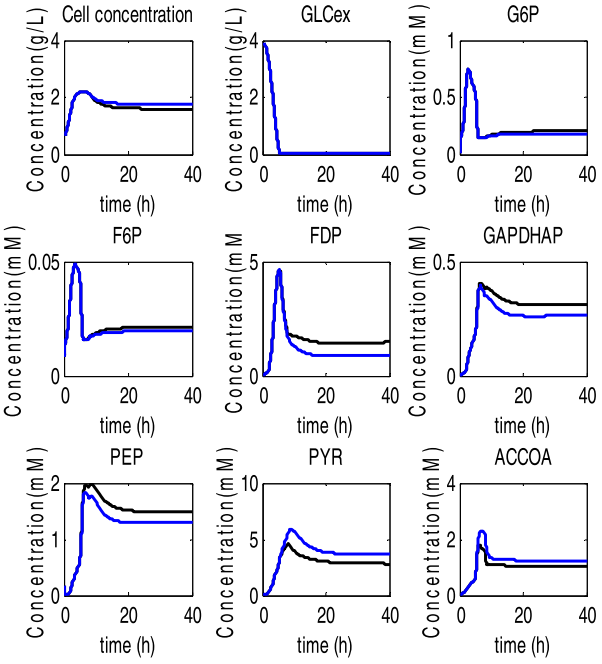

FIGURE 15. $k^{d}_{icdhnadp}$ changes on the model response.

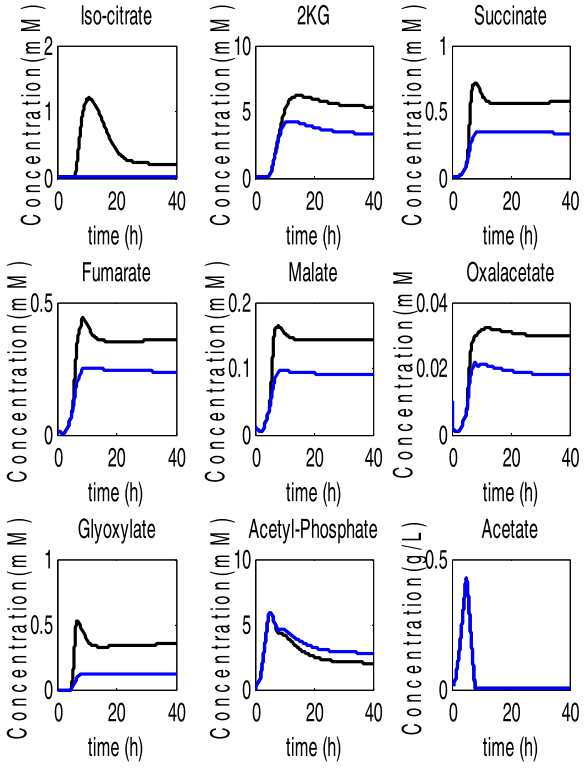

FIGURE 16. $k^{d}_{icdhnadp}$ changes on the model response.

simultaneously toward metabolite error minimization using real experimental data. The kinetic parameter identification was achieved and is presented in Table 2 with upper, lower and optimized values based on the model kinetic

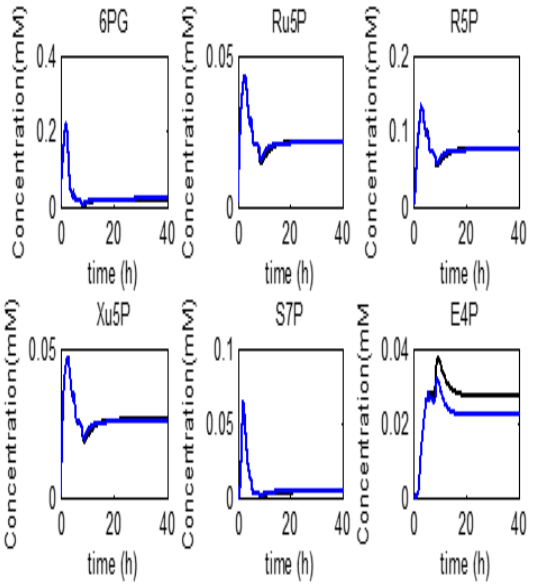

FIGURE 17. $k^{d}_{icdhnadp}$ changes on the model response.

TABLE 2. The model simulation.

KINETICS	ORIGINAL	LOWER	UPPER	OPTIMIZE
v^{pyk}_{max}	1.085	0.9	1.34	1.063
n_{pk}	3	2.5	3.25	3.09
$icdhh$	24.421	23.9	24.6	24.47
k^{f}_{icdh}	289800	289799.4	289800.5	289799.9
$k^{d}_{icdhnadp}$	0.006	0.004	0.04	0.0085
$k^{m}_{icdhndap}$	0.017	0.009	0.019	0.0169
v^{icl}_{max}	3.8315	3.3315	4.1	3.79
v^{pyk}_{max}	1.085	0.9	1.34	1.063
n_{pk}	3	2.5	3.25	3.09

parameters values. The algorithm optimized the metabolites well, as described in Table 3. In the model under investigation, the increasing $2KG$ production as seen above in the results of [25] by the identification is minimized with reasonable effects, either increasing or decreasing, on the other metabolites and thus might be because of the affection of OAA, requiring building the anaplerotic pathway [25]. Moreover, during PSO adoption execution, the error minimization of the GLc, PYR, and $AcCOA$ metabolites was increased compared to the experimental values; where the metabolites of $DHAP/GAP$, FDP, PEP, $6PG$, $2KG$ and Ace were very close to the experimental values and were almost same. On the contrary, the other metabolites were moved toward experimental data with small errors. These changes occurred and might be due to the participation of other metabolites, a lack of experimental data, model complexity, and the lumping of some metabolites to simplify the model. However, the model error minimization after adopting the PSO algorithm is described in Figure 24 to compare the model under study

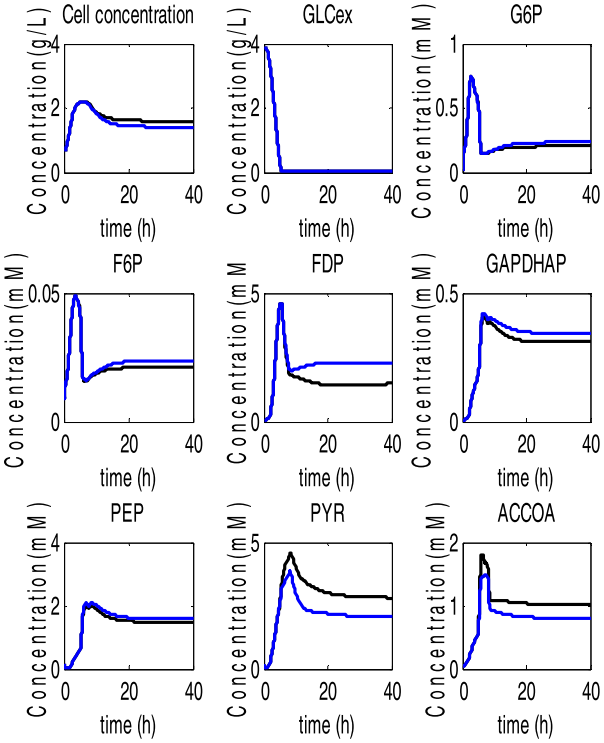

FIGURE 18. $k^{m}_{icdhnadp}$ changes on the model response.

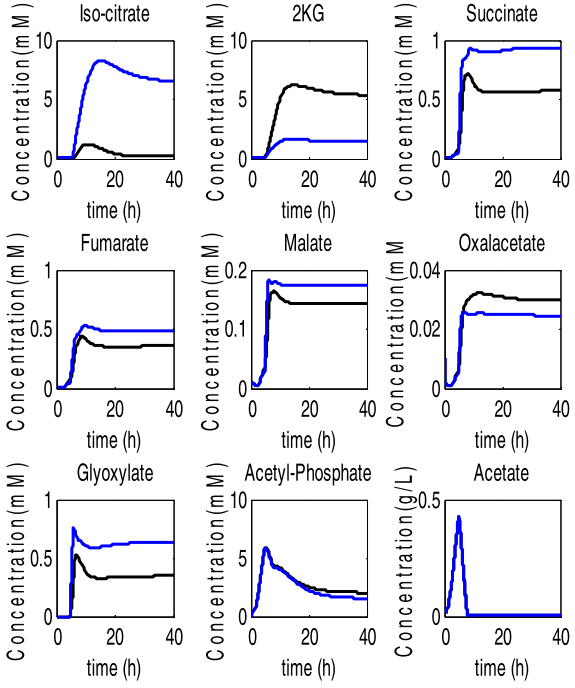

FIGURE 19. $k^{m}_{icdhnadp}$ changes on the model response.

and the simulation result of the main metabolic model of *E. coli* using real experimental data from [27], which were achieved in 23 h.

TABLE 3. The model simulation.

Metabolites	Hoque Experimental	Kadir Simulation	Optimized Values Se-PSO	Optimized Values PSO
Glc	0.0617	0.12276	0.20195	0.16717
$G6P$	1.76	0.20364	0.17731	0.18432
$F6P$	0.42	0.02132	0.01906	0.019671
$DHAP/GAP$	0.231	0.31106	0.23518	0.24961
FDP	0.67	1.4645	0.71747	0.84333
PEP	1.04	1.4917	1.1587	1.2159
PYR	1.71	2.8101	3.832	3.3025
$6PG$	0.96	0.01785	0.01881	0.018278
$Ribu5P$	0.088	0.02135	0.02101	0.020927
$Rib5P$	0.243	0.0762	0.07457	0.074428
$E4P$	0.112	0.02744	0.02003	0.021616
$AcCoA$	0.145	1.0015	1.2679	1.117
OAA	0.241	0.02962	0.01592	0.022679
ICT	0.21	0.2103	0.00206	0.012406
$2KG$	0.134	5.3656	2.8222	4.2219
Ace	0.36	0.00347	0.00626	0.0049875

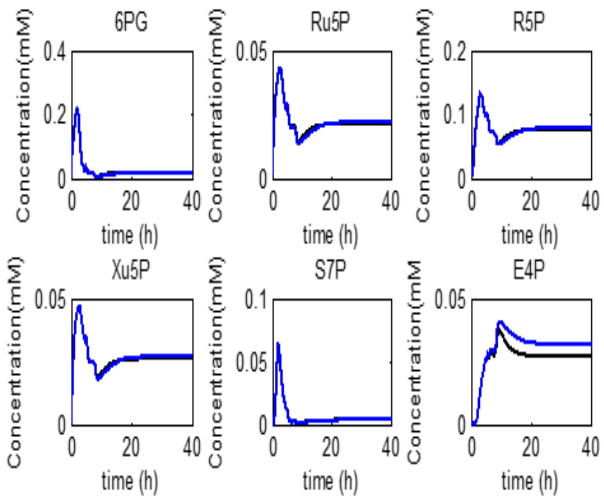

FIGURE 20. $k^{m}_{icdhnadp}$ changes on the model response.

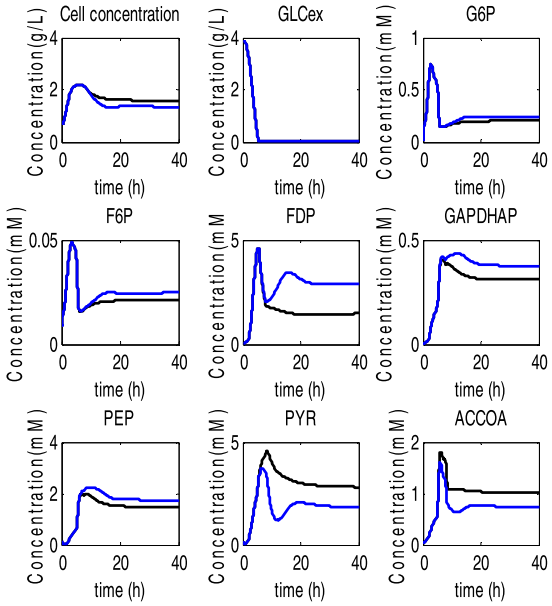

FIGURE 21. v^{icl}_{max} changes on the model response.

C. THE Se-PSO RESULT

In the Se-PSO algorithm, the whole mass balance equations described by (ODE) and reaction rates, including the whole kinetic parameters, were adopted, starting by adopting the seven parameter boundaries based on the kinetic parameter simulation values of the model under study and were found during PSO execution toward model minimization. During Se-PSO adoption execution, the calculation value of each parameter was determined simultaneously toward metabolite minimization using real experimental datah

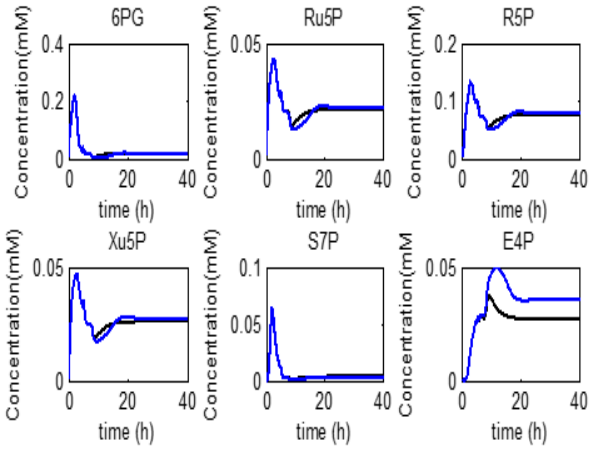

FIGURE 22. v_{max}^{icl} changes on the model response.

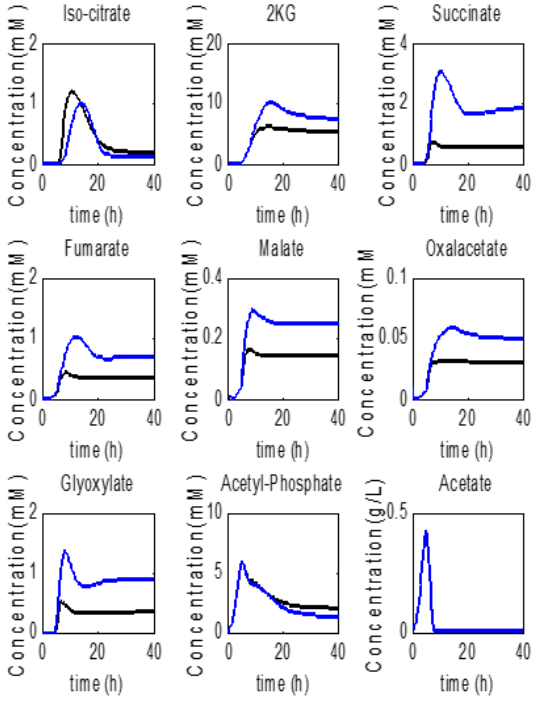

FIGURE 23. v_{max}^{icl} changes on the model response.

TABLE 4. The segmentation.

KINETICS	NUMBER OF SEGMENTS
v_{max}^{pyk}	1
n_{pk}	2
$icdh$	1
k_{icdh}^{f}	1
$k_{icdhnap}^{d}$	2
$k_{icdhnap}^{m}$	1
v_{max}^{icl}	2

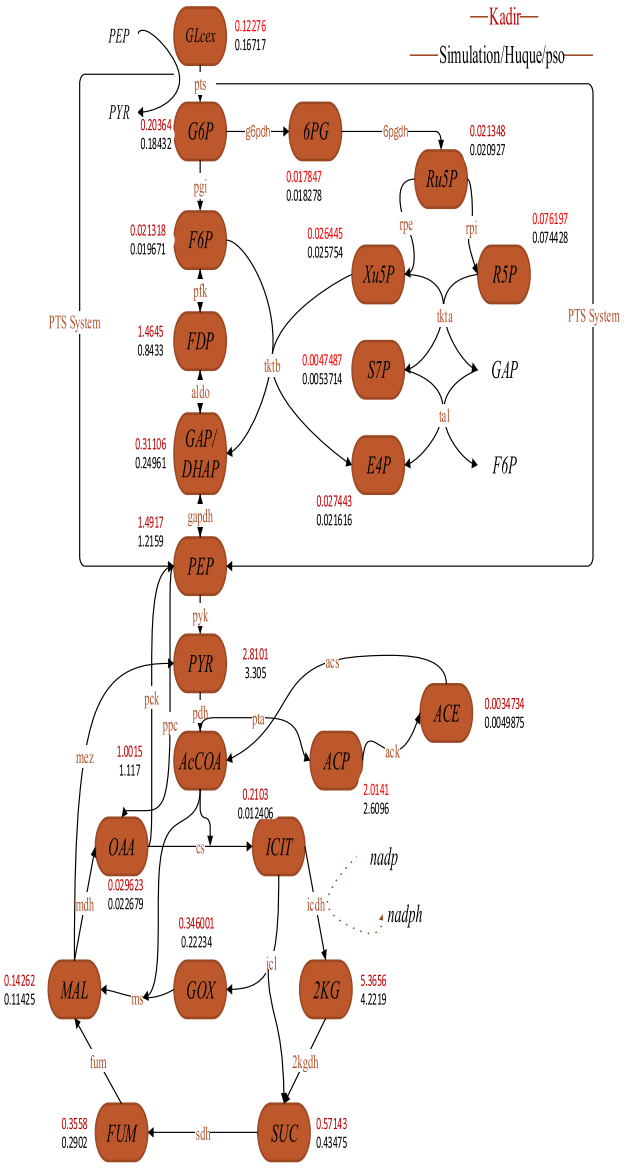

FIGURE 24. The simulation result with model result.

TABLE 5. Se-PSO kinetic parameters identification.

KINETICS	ORIGINAL	LOWER	UPPER	OPTIMIZE
v_{max}^{pyk}	1.085	0.9	1.34	0.989
n_{pk}	3	2.5	3.25	3.1
$icdh$	24.421	23.9	24.6	24.09625
k_{icdh}^{f}	289800	289799.4	289800.5	289799.8
$k_{icdhnadp}^{d}$	0.006	0.004	0.04	0.028798
$k_{icdhnadp}^{m}$	0.017	0.009	0.019	0.013343
v_{max}^{icl}	3.8315	3.3315	4.1	3.787502

parameter was determined simultaneo by Equation (3). The number of segments used in this adoption is described in Table 4 in addition to the identification of 7 kinetic parameters with their upper and lower boundaries, which is shown in Table 5 below based on the sensitivity affection on the model response. However, segmentation was proposed based on the sensitivity analysis affection result of the kinetic parameters.

TABLE 6. The model simulation.

Metabolites	Hoque Experimental	Kadir Simulation	Optimized Values Se-PSO	Optimized Values PSO
Glc	0.0617	0.12276	0.20195	0.16717
$G6P$	1.76	0.20364	0.17731	0.18432
$F6P$	0.42	0.02132	0.01906	0.019671
$DHAP/GAP$	0.231	0.31106	0.23518	0.24961
FDP	0.67	1.4645	0.71747	0.84333
PEP	1.04	1.4917	1.1587	1.2159
PYR	1.71	2.8101	3.832	3.3025
$6PG$	0.96	0.01785	0.01881	0.018278
$Ribu5P$	0.088	0.02135	0.02101	0.020927
$Rib5P$	0.243	0.0762	0.07457	0.074428
$E4P$	0.112	0.02744	0.02003	0.021616
$AcCoA$	0.145	1.0015	1.2679	1.117
OAA	0.241	0.02962	0.01592	0.022679
ICT	0.21	0.2103	0.00206	0.012406
$2KG$	0.134	5.3656	2.8222	4.2219
Ace	0.36	0.00347	0.00626	0.0049875

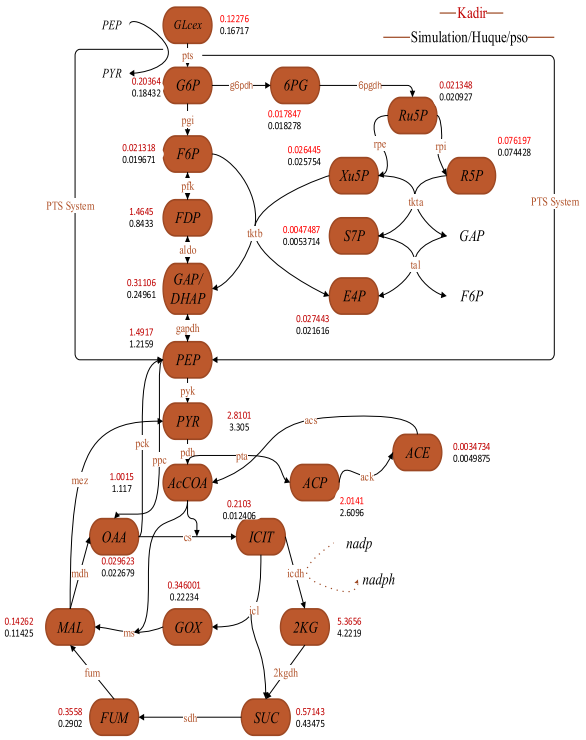

FIGURE 25. The simulation result with the model result.

Kinetic parameter identification was achieved and is presented in Table 5 with upper, lower and optimized values based on the model kinetic parameter values, while the algorithm optimized the metabolites well, as described in Table 6.

In the model under investigation in Table 6, there were substantial increases in $2KG$ production as seen above in the results of [25], whereby the identification was minimized well in PSO and Se-PSO with reasonable increases or decreases in the other metabolites. This may be because of the affection of OAA required to build the *anaplerotic* pathway [25]. In addition, Se-PSO achieved better identification. Moreover, during the Se-PSO adoption execution, the error minimization of the GLc, PYR, and $AcCOA$ metabolites increased highly compared to the experimental values; however, the metabolites of $DHAP/GAP$, $Ribu5P$, $Rib5P$, FDP, PEP, $6PG$, $2KG$, and Ace were very close to the experimental values and were almost the same. On the contrary, the other metabolites were moved toward the experimental data slightly with small errors. These changes occurred due to the participation of other metabolites, a lack of experimental data, model complexity, glucose depletion, and the lumping of some metabolites to simplify the model.

Moreover, the result of the PSO and Se-PSO algorithms were compared, and it can be seen clearly that Se-PSO was moving the simulation result toward the experimental data by minimizing the errors compared to the PSO adoption result for 21 h. However, the model error minimization after adopting the Se-PSO algorithm is described in Figure 25 above compared to the model under study and the simulation result

TABLE 7. Kinetic rate equations.

Reaction's	Kinetic equation	References
Cell growth (X)	$\begin{cases} \mu_m\left(1-\frac{[X]}{X_m}\right)\left(\frac{[GLc^{ex}]}{K_s+[GLc^{ex}]}\right)k_{ATP}v_{ATP}(.), ([GLc^{ex}]>0) \\ \frac{\mu_{mA}[Ace^{ex}]}{K_{sA}+[Ace^{ex}]}\ k_{ATP}v_{ATP}(.), ([GLc^{ex}]\le 1\ and [Ace^{ex}]>0) \end{cases}$	25
PTS (Phosphotransferase system)	$\frac{v_{PTS}^{max}[GLc^{ex}]\frac{[PEP]}{PYR}}{\left(K_{a1}+K_{a2}\frac{[PEP]}{[PYR]}+K_{a3}[GLc^{ex}]+[GLc^{ex}]\frac{[PEP]}{[PYR]}\right)\left(1+\frac{[G6P]^nG6P}{K_{G6P}}\right)}$	25
PGI (Phosphoglucoseisomerase)	$\frac{v_{PGI}^{max}\left([G6P]-\frac{[F6P]}{Keq}\right)}{K_{G6P}\left(1+\frac{[F6P]}{K_{F6P}\left(1+\frac{[F6P]}{K_{6pginh}^{F6P}}\right)}+\frac{[6PG]}{K_{6pginh}^{G6P}}\right)+G6P}$	25
PFK (Phospho-fructokinase)	$\frac{v_{PFK}^{max}K_{ATP}[F6P]}{K_{(ATP,ADP)}\left([F6P]+K_z^{F6P}\frac{K_{b(ADP,AMP)}+\frac{[PEP]}{K_{PEP}}}{K_{a(ADP,AMP)}}\right)\left(1+\frac{L_{pfk}}{\left(1+[F6P]\left(\frac{K_{a(ADP,AMP)}}{K_S^{F6P}\left(K_{b(ADP,AMP)}+\frac{[PEP]}{K_{PEP}}\right)}\right)\right)^{n_{PFK}}}\right)}$	25
Aldo (Adolase)	$\frac{v_{ALDO}^{max}\left([FDP]-\frac{[DHAP][GAP]}{Keq}\right)}{\left(K_{FDP}+[FDP]+\frac{K_{GAP}[DAHP]}{[K_{eq}V_{bif}]}+\frac{K_{DHAP}[GAP]}{[K_{eq}V_{bif}]}+\frac{[FDP][GAP]}{K_{inh}^{PEP}}+\frac{[DHAP][GAP]}{K_{eq}V_{bif}}\right)}$	25
GAPDH (Glyceraldehyde 3-phosphate dehydrogenase)	$\frac{v_{GAPDH}^{max}\left([GAP]-\frac{[PEP][NADH]}{Keq[NAD]}\right)}{\left(K_{GAP}\left(1+\frac{[PEP]}{K_{PGP}}\right)+[GAP]\right)\left(\frac{K_{NAD}}{NAD}\left(1+\frac{[NADH]}{K_{NADH}}\right)+1\right)}$	25
PYK (Pyruvate kinase)	$\frac{v_{PYK}^{max}[PEP]\left(\frac{PEP}{K_{PEP}}+1\right)^{n_{pyk}-1}[ADP]}{K_{PEP}\left(L_{PYK}\left(\frac{1+\frac{[ATP]}{K_{ATP}}}{\frac{[FDP]}{K_{FDP}}+\frac{[AMP]}{K_{AMP}}+1}\right)^{n_{pyk}}+\left(\frac{[PEP]}{K_{PEP}}+1\right)^{n_{pyk}}\right)([ADP]+K_{ADP})}$	25
Ppc (PEP carboxylase)	$\frac{K_1+K_2[AcCOA]+K_3[FDP]+K_4[AcCOA][FDP]}{1+K_5[AcCOA]+K_6[FDP]}\left(\frac{[PEP]}{K_m+[PEP]}\right)$	25
G6PDH	$\frac{v_{G6PDH}^{max}[G6P][NADP]}{([G6P]+K_{g6p})\left(1+\frac{[NADPH]}{K_{ndph}}\right)\left(K_{nadp}\left(1+\frac{[NADPH]}{K_{nadph}}\right)+NADP\right)}$	25
PGDH (Phosphogluconate Dehydrogenase)	$\frac{v_{PGDH}^{max}[6PG][NADP]}{([6PG]+K_{6pg})\left([NADP]+K_{nadp}\left(1+\frac{[NADPH]}{K_{nadph}}\right)\left(1+\frac{[ATP]}{K_{atp}}\right)\right)}$	25
Rpe (Ribulose-phosphate 3-epimerase)	$v_{Rpe}^{max}\left([Ru5P]-\frac{[R5P]}{K_{eq}^{Rpe}}\right)$	25
Rpi (ribose-5-phosphate isomerase)	$v_{Rpi}^{max}\left([Ru5P]-\frac{[R5P]}{K_{eq}^{Rpi}}\right)$	25
TktA (transketolase A)	$v_{TKtA}^{max}\left([R5P][Xu5P]-\frac{[S7P][GAP]}{K_{eq}^{TKtA}}\right)$	25

TABLE 7. ***(Continued.)*** **Kinetic rate equations.**

TktB (transketolase B)	$v_{TKtB}^{max}\left([Xu5P][E4P]-\frac{[F6P][GAP]}{K_{eq}^{TKtB}}\right)$	25
Tal (Tyrosine ammonia lyase)	$v_{TaL}^{max}\left([GAP][S7P]-\frac{[E4P][F6P]}{K_{eq}^{TKtB}}\right)$	25
PcK (PEP carboxykinase)	$v_{PcK}^{max}\left(\frac{[OAA]\frac{[ATP]}{[ADP]}}{K_m^{OAA}\frac{[ATP]}{[ADP]}+[OAA]\frac{[ATP]}{[ADP]}+\frac{K_i^{ATP}K_m^{OAA}}{K_i^{ADP}}+\frac{K_i^{ATP}K_m^{OAA}}{K_m^{PEP}K_i^{ADP}}[PEP]+\frac{K_i^{ATP}K_m^{OAA}}{K_i^{PEP}K_l^{ATP}}\frac{[ATP][PEP]}{[ADP]}+\frac{K_i^{ATP}K_m^{OAA}}{K_i^{ADP}K_l^{OAA}}[OAA]}\right)$	25
PDH (Pyruvate dehydrogenase complex)	$\frac{\frac{v_{PDH}^{max}}{[NAD]}\left(\frac{1}{1+K_i\frac{[NADH]}{[NAD]}}\right)\left(\frac{[PYR]}{K_m^{PYR}}\right)\left(\frac{1}{K_m^{NAD}}\right)\left(\frac{[COA]}{K_m^{COA}}\right)}{\left(1+\frac{[PYR]}{K_m^{PYR}}\right)\left(\frac{1}{NAD}+\frac{1}{K_m^{NAD}}+\frac{[NADH]}{K_m^{NADH}[NAD]}\right)\left(1+\frac{[COA]}{K_m^{COA}}+\frac{[AcCOA]}{K_m^{AcCOA}}\right)}$	25
Pta (Phosphotransacetylase)	$\frac{v_{Pta}^{max}\left(\frac{1}{K_i^{AcCOA}K_m^{P}}\right)\left([AcCoA][P]-\frac{[AcP][CoA]}{K_{eq}}\right)}{\left(1+\frac{[AcCoA]}{K_i^{AcCOA}}+\frac{[P]}{K_i^{P}}+\frac{[ACP]}{K_i^{ACP}}+\frac{[CoA]}{K_i^{CoA}}+\left(\frac{[AcCoA][P]}{K_i^{AcCOA}K_m^{P}}\right)+\left(\frac{[AcP][CoA]}{K_m^{ACP}K_i^{CoA}}\right)\right)}$	25
Ack (Acetate kinase)	$\frac{v_{Ack}^{max}\left(\frac{1}{K_m^{ADP}K_m^{ACP}}\right)\left([AcP][ADP]-\frac{[ACE][ATP]}{K_{eq}}\right)}{\left(1+\frac{[Acp]}{K_m^{ACP}}+\frac{[ACE]}{K_m^{ACE}}\right)\left(1+\frac{[ADP]}{K_m^{ADP}}+\frac{[ATP]}{K_m^{ATP}}\right)}$	25
Acs (acyl-coenzyme A synthetase)	$\frac{v_{Acs}^{max}[ACE][NADP]}{(K_m+[ACE])(K_{eq}+[NADP])}$	25
Cs (Citrate Synthase)	$\frac{v_{CS}^{max}[AcCoA][OAA]}{(K_d^{AcCoA}K_m^{OAA}+K_m^{AcCoA}[OAA])+\left([AcCoA]K_m^{OAA}\left(1+\frac{[NADH]}{K_{i1}^{NADH}}\right)\right)+\left([AcCoA][OAA]\left(1+\frac{[NADH]}{K_{i2}^{NDAH}}\right)\right)}$	25
ICDH (Isocitrate dehydrogenase)	$\frac{[ICDH]\frac{K_f}{K_m^{ICIT}}K_d^{NADP}\left([ICIT]-\frac{[NADH][2KG]}{K_{eq}^{ICDH}[NADP]}\right)}{\left(\begin{array}{l}\frac{1}{[NADP]}+\frac{[ICIT]K_m^{NADP}}{K_m^{ICIT}K_d^{NADP}[NADP]}+\frac{1}{K_d^{NADP}}+\frac{[ICIT]}{K_m^{ICIT}K_d^{NADP}}+\frac{[ICIT]}{K_d^{ICIT}[NADP]}\frac{[NADPH]K_m^{NADP}}{K_m^{ICIT}K_m^{NADP}K_{einh}^{NADPH}}+\\ \frac{[NADPH]K_{eknh}^{2KG}}{K_m^{2KG}K_{enhe}^{NADPH}[NADP]}+\frac{[2KG]K_m^{NADPH}}{K_m^{2KG}K_{enhe}^{NADPH}[NADP]}+\frac{[2KG]}{K_m^{2KG}}\frac{[NADPH]}{K_{enhe}^{NADPH}[NADP]}+\frac{[2KG]K_m^{NADPH}}{K_m^{2KG}K_m^{NADPH}}\frac{[NADPH]}{K_{ekn}^{NADP}[NADP]}\end{array}\right)}$	25
IcL (Isocitrate lyase)	$\frac{v_{lcl-f}^{max}\frac{[ICIT]}{K_m^{ICIT}}}{\left(1+\frac{[ICIT]}{K_m^{ICIT}}+\frac{[SUC]}{K_m^{SUC}}+\frac{[PEP]}{K_m^{PEP}}+\frac{[2KG]}{K_m^{2KG}}+\frac{1}{K_l}\right)}$	25
MS (Malate synthase)	$\frac{v_{MS}^{max}\frac{[GOX]}{K_m^{GOX}}\frac{[AcCoA]}{K_m^{AcCOA}}-v_{MS}^{max}\frac{[MAL]}{K_m^{MAL}}}{\left(1+\frac{[GOX]}{K_m^{GOX}}+\frac{[MAL]}{K_m^{MAL}}+\left(1+\frac{[AcCoA]}{K_m^{AcCOA}}\right)\right)}$	25
aKGDH (aKG dehydrogenase)	$\frac{v_{2KGDH}^{max}[aKG][CoA]}{\left(\begin{array}{l}\frac{K_m^{NAD}[aKG][CoA]}{[NAD]}+K_m^{CoA}[aKG]+K_m^{2KG}[CoA]+[aKG][CoA]+\frac{K_m^{2KG}K_Z[aKG][SUC][NADH]}{K_1^{2KG}K_1^{SUC}[NAD]}\\ \frac{K_m^{2KG}K_Z[SUC][NADH]}{K_1^{SUC}[NAD]}+\frac{K_m^{NAD}[aKG][CoA][NADH]}{K_1^{NADH}[NAD]}+\frac{K_m^{CoA}[aKG][SUC]}{K_1^{SUC}}\end{array}\right)}$	25
SDH (Succinate dehydrogenase)	$\frac{v_{SDH1}v_{SDH2}\left([SUC]-\frac{[FUM]}{K_{eq}}\right)}{K_m^{SUC}v_{SDH2}+v_{SDH2}[SUC]+\frac{v_{SDH1}[FUM]}{K_{eq}}}$	25
Fum (Fumarase)	$\frac{v_{Fum1}v_{Fum2}\left([FUM]-\frac{[MAL]}{k_{Fum\,eq}}\right)}{K_m^{Fum}v_{Fum1}+v_{Fum2}[FUM]+\frac{V_{Fum1}[MAL]}{K_{eq}}}$	25

TABLE 7. *(Continued.)* **Kinetic rate equations.**

Mez (Malic enzyme)	$\frac{v_{Mez}^{max}\,[MAL]\,[NADP]}{(K_{MAL}+[MAL])\,(K_{eq}+[NADP])}$	25
MDH (Malate dehydrogenase)	$\frac{v_{MDH1}v_{MDH2}\left([MAL]-\frac{[OAA]}{K_{eq}}\right)}{\left(\begin{array}{c}\frac{K_1^{NAD}K_m^{MAL}v_{MDH2}}{[NAD]}+K_m^{MAL}\,v_{MDH2}+\frac{K_m^{NAD}v_{MDH2}[MAL]}{[NAD]}+v_{MDH2}[MAL]+\frac{K_m^{OAA}v_{MDH1}[NADH]}{K_{eq}[NAD]}+\frac{K_m^{NADH}v_{MDH1}[OAA]}{K_{eq}[NAD]}+\\ \frac{v_{MDH1}[NADH][OAA]}{K_{eq}[NAD]}+\frac{v_{MDH1}K_m^{OAA}[NADH]}{K_{eq}K_1^{NAD}}+\frac{v_{MDH2}K_m^{NAD}[MAL][OAA]}{K_1^{OAA}[NAD]}+\frac{v_{MDH2}[MAL][NADH]}{K_1^{NAD}}\\ +\frac{v_{MDH1}[MAL][NADH][OAA]}{K_{eq}K_1^{MAL}[NAD]}+\frac{v_{MDH2}[MAL][OAA]}{K_{II}^{OAA}}+\frac{v_{MDH1}[NADH][OAA]}{K_{II}^{NAD}K_{eq}}+\frac{K_1^{NAD}v_{MDH2}[MAL][NADH][OAA]}{K_{II}^{NAD}K_m^{OAA}K_1^{NADH}}\end{array}\right)^2}$	25

of the main metabolic model of *E. coli* using real experimental data taken from [29].

IV. CONCLUSION

Large-scale kinetic parameters were used as a targeted study for efficiency identification in the main dynamic metabolic network under the steady-state condition of *E. coli* experimentally by programming how much they affect the model response, minimizing errors with respect to the real experimental data. Seven kinetic parameters were the most effective ones described in detail. The Segmentation Particle Swarm Optimization Algorithm and Particle Swarm Optimization were adopted to identify the kinetics under study using the dynamic model containing an ODE function tuned based on continuous culture with a dilution rate 0.1 to minimize the model response error. The Se-PSO and PSO algorithms moved the model responses toward the experimental data and clearly showed that Se-PSO was performing better than PSO. To this point, identification was achieved with optimum results. This adoption of the PSO and Se-PSO algorithm efficiency solves the large-scale kinetic parameter identification due to the convergence speed and time consumption for each algorithm. Moreover, the whole kinetic system needs further study by optimizing the v^{max} parameters with the 7th kinetic parameter sensitivity analysis result achieved so far in this study. Finally, the adoption of other algorithms, such as the African Buffalo Optimization, artificial bee colony algorithm and the Segmentation of African Buffalo Optimization and artificial bee colony algorithm, will be considered in the future.

APPENDIX

See Table 7.

ACKNOWLEDGMENT

The authors would like to thank Dr. Tuty Asmawaty Abdul Kadir, who supervised this work.

REFERENCES

[1] S. M. Baker, C. H. Poskar, F. Schreiber, and B. H. Junker, "A unified framework for estimating parameters of kinetic biological models," *BMC Bioinform.*, vol. 16, no. 1, p. 104, 2015.
[2] A. Degasperi, D. Fey, and B. N. Kholodenko, "Performance of objective functions and optimisation procedures for parameter estimation in system biology models," *NPJ Syst. Biol. Appl.*, vol. 3, no. 1, p. 20, 2017.
[3] R. N. Krishnaraj and P. Pal, "Enzyme-substrate interaction based approach for screening electroactive microorganisms for microbial fuel cell applications," *Indian J. Chem. Technol.*, vol. 24, pp. 93–96, Jan. 2017.
[4] A. Gábor, A. F. Villaverde, and J. R. Banga, "Parameter identifiability analysis and visualization in large-scale kinetic models of biosystems," *BMC Syst. Biol.*, vol. 11, no. 1, p. 54, 2017.
[5] T. Aho, O. P. Smolander, J. Niemi, and O. Yli-Harja, "RMBNToolbox: random models for biochemical networks," *BMC Syst. Biol.*, vol. 1, no. 1, p. 22, 2007.
[6] D. Vercammen, F. Logist, and J. Van Impe, "Dynamic estimation of specific fluxes in metabolic networks using non-linear dynamic optimization," *BMC Syst. Biol.*, vol. 8, no. 1, p. 132, 2014.
[7] J. Yang *et al.*, "Metabolic engineering of *Escherichia coli* for the biosynthesis of alpha-pinene," *Biotechnol. Biofuels*, vol. 6, no. 1, p. 60, 2013.
[8] N. Ishii *et al.*, "Dynamic simulation of an *in vitro* multi-enzyme system," *FEBS Lett.*, vol. 581, no. 3, pp. 413–420, 2007.
[9] G. Guillén-Gosálbez, A. Miró, R. Alves, A. Sorribas, and L. Jiménez, "Identification of regulatory structure and kinetic parameters of biochemical networks via mixed-integer dynamic optimization," *BMC Syst. Biol.*, vol. 7, no. 1, p. 113, 2013.
[10] C. Zhan, W. Situ, L. F. Yeung, P. W.-M. Tsang, and G. Yang, "A parameter estimation method for biological systems modelled by ODE/DDE models using spline approximation and differential evolution algorithm," *IEEE/ACM Trans. Comput. Biol. Bioinf.*, vol. 11, no. 6, pp. 1066–1076, Nov. 2014.
[11] D. A. Shelley, B. L. Sih, and L. J. Ng, "An integrated physiology model to study regional lung damage effects and the physiologic response," *Theor. Biol. Med. Model.* , vol. 11, no. 1, p. 32, 2014.
[12] Y. Tohsato, K. Ikuta, A. Shionoya, Y. Mazaki, and M. Ito, "Parameter optimization and sensitivity analysis for large kinetic models using a real-coded genetic algorithm," *Gene*, vol. 518, no. 1, pp. 84–90, 2013.
[13] C. Chassagnole, N. Noisommit-Rizzi, J. W. Schmid, K. Mauch, and M. Reuss, "Dynamic modeling of the central carbon metabolism of *Escherichia coli*," *Biotechnol. Bioeng.*, vol. 79, no. 1, pp. 53–73, 2002.
[14] J. Di Maggio, J. C. D. Ricci, and M. S. Diaz, "Parameter estimation in kinetic models for large scale metabolic networks with advanced mathematical programming techniques," *Comput. Aided Chem. Eng.*. vol. 28, pp. 355–360, Jan. 2010.
[15] A. L. Campos, J. Nogueira, F. A. Coelho, A. M. F. Fileti, and B. F. Santos, "Genetic algorithm optimization of the parameters involved in biosurfactant production from beet peel as substrate," *Chem. Eng. Trans.*, vol. 65, pp. 469–474, Jun. 2018.
[16] M. A. Abido, "Multiobjective particle swarm optimization for environmental/economic dispatch problem," *Electr. Power Syst. Res.*, vol. 79, no. 7, pp. 1105–1113, 2009.
[17] M. A. Kunna, T. A. A. Kadir, A. S. Jaber, and J. B. Odili, "Large-scale kinetic parameter identification of metabolic network model of *E. coli* using PSO," *Adv. Biosci. Biotechnol.*, vol. 6, no. 2, p. 120, 2015.
[18] R. Eberhart and J. Kennedy, "A new optimizer using particle swarm theory," in *Proc. 6th Int. Symp. IEEE Micro Mach. Hum. Sci. (MHS)*, Oct. 1995, pp. 39–43.

[19] A. S. Jaber, A. Z. Ahmad, and A. N. Abdalla, "An investigation of scaled-FLC using PSO for multi-area power system load frequency control," *Energy Power Eng.*, vol. 5, no. 4, p. 458, 2013.
[20] S. Zhang, H. Jiang, Y. Yin, W. Xiao, and B. Zhao, "The prediction of the gas utilization ratio based on TS fuzzy neural network and particle swarm optimization," *Sensors*, vol. 18, no. 2, p. 625, 2018.
[21] M. Ghovvati, G. Khayati, H. Attar, and A. Vaziri, "Kinetic parameters estimation of protease production using penalty function method with hybrid genetic algorithm and particle swarm optimization," *Biotechnol. Biotechnol. Equip.*, vol. 30, no. 2, pp. 404–410, 2016.
[22] A. Tarique and H. A. Gabbar, "Particle swarm optimization (PSO) based turbine control," *Intell. Control Automat.* , vol. 4, no. 2, pp. 126–137, 2013.
[23] A. S. Jaber, A. Z. Ahmad, and A. Abdalla, "A new parameters identification of single area power system based LFC using segmentation particle swarm optimization (SePSO) algorithm," in *Proc. IEEE PES Asia–Pacific Power Energy Eng. Conf. (APPEEC)*, Dec. 2013, pp. 1–6.
[24] U. Khaled, A. M. Eltamaly, and A. Beroual, "Optimal power flow using particle swarm optimization of renewable hybrid distributed generation," *Energies*, vol. 10, no. 7, p. 1013, 2017.
[25] T. A. Kadir, A. A. Mannan, A. M. Kierzek, J. McFadden, and K. Shimizu, "Modeling and simulation of the main metabolism in *Escherichia coli* and its several single-gene knockout mutants with experimental verification," *Microbial Cell Factories*, vol. 9, no. 1, p. 88, 2010.
[26] C. Farber, J. L. Neary, T. G. Lilburn, and Y. Wang, "Metabolic pathway complements of eight *Escherichia coli* strains," in *Proc. IEEE Int. Conf. Bioinform. Biomed. Workshops (BIBMW)*, Nov. 2008, pp. 127–131.
[27] M. Kotera and S. Goto, "Metabolic pathway reconstruction strategies for central metabolism and natural product biosynthesis," *Biophys. Physicobiol.*, vol. 13, pp. 195–205, Jul. 2016.
[28] Y. Deville, D. Gilbert, J. Van Helden, and S. J. Wodak, "An overview of data models for the analysis of biochemical pathways," *Briefings Bioinform.*, vol. 4, no. 3, pp. 246–259, 2003.
[29] A. Hoque, H. Ushiyama, M. Tomita, and K. Shimizu, "Dynamic responses of the intracellular metabolite concentrations of the wild type and *pyk*A mutant *Escherichia coli* against pulse addition of glucose or NH_3 under those limiting continuous cultures," *Biochem. Eng. J.*, vol. 26, no. 1, pp. 38–49, 2005.
[30] S.-C. Fang, B.-R. Ke, and C.-Y. Chung, "Minimization of construction costs for an all battery-swapping electric-bus transportation system: Comparison with an all plug-in system," *Energies*, vol. 10, no. 7, p. 890, 2017.

MOHAMMED ADAM KUNNA AZRAG received the B.Sc. degree (Hons.) in computer studies from the National Ribat University, in 2010, and the M.Sc. degree in computer science from Universiti Malaysia Pahang, in 2015, where he is currently pursuing the Ph.D. degree. His research interests include optimization algorithms and data base.

TUTY ASMAWATY ABDUL KADIR was born in Pahang, Malaysia, in 1976. She received the B.Sc. degree (Hons.) in computer science and the M.Sc. degree in computer science from the University Technology of Malaysia, Malaysia, in 1999 and 2005, respectively, and the Ph.D. degree in engineering (information science) from the Kyushu Institute of Technology, Japan, in 2010. Since 2002, she has been a Senior Lecturer with Universiti Malaysia Pahang, Malaysia. Her research interests include modeling and simulation, serious games, and image processing.

AQEEL S. JABER was born in Baghdad, Iraq, in 1977. He received the B.E. and M.E. degrees from the University of Technology, Bagdad, Iraq, in 2001 and 2007, respectively, and the Ph.D. degree from Universiti Malaysia Pahang, Pahang, Malaysia, in 2015.

Since 2009, he has been holding lecturing positions at the Department of Electrical Power Engineering Techniques, Al-Mamon University College, Baghdad, where he is currently a Senior Lecturer.